Validation and Parametric Investigations Using a Lumped Thermal Parameter Model of an Internal Permanent Magnet Motor

Preprint

Sebastien Sequeira,[1] Kevin Bennion,[2] J. Emily Cousineau,[2] Sreekant Narumanchi,[2] Gilbert Moreno,[2] Satish Kumar,[1] and Yogendra Joshi[1]

1 Georgia Institute of Technology
2 National Renewable Energy Laboratory

Presented at the ASME 2020 International Technical Conference and Exhibition on Packaging and Integration of Electronic and Photonic Microsystems (InterPACK2020)
October 27-29, 2020

NREL is a national laboratory of the U.S. Department of Energy
Office of Energy Efficiency & Renewable Energy
Operated by the Alliance for Sustainable Energy, LLC

This report is available at no cost from the National Renewable Energy Laboratory (NREL) at www.nrel.gov/publications.

Contract No. DE-AC36-08GO28308

Conference Paper
NREL/CP-5400-77082
October 2020

Validation and Parametric Investigations Using a Lumped Thermal Parameter Model of an Internal Permanent Magnet Motor

Preprint

Sebastien Sequeira,[1] Kevin Bennion,[2] J. Emily Cousineau,[2] Sreekant Narumanchi,[2] Gilbert Moreno,[2] Satish Kumar,[1] and Yogendra Joshi[1]

1 Georgia Institute of Technology
2 National Renewable Energy Laboratory

Suggested Citation
Sequeira, Sebastien, Kevin Bennion, J. Emily Cousineau, Sreekant Narumanchi, Gilbert Moreno, Satish Kumar, Yogendra Joshi. 2020. *Validation and Parametric Investigations Using a Lumped Thermal Parameter Model of an Internal Permanent Magnet Motor: Preprint*. Golden, CO: National Renewable Energy Laboratory. NREL/CP-5400-77082. https://www.nrel.gov/docs/fy21osti/77082.pdf.

NREL is a national laboratory of the U.S. Department of Energy
Office of Energy Efficiency & Renewable Energy
Operated by the Alliance for Sustainable Energy, LLC

This report is available at no cost from the National Renewable Energy Laboratory (NREL) at www.nrel.gov/publications.

Contract No. DE-AC36-08GO28308

Conference Paper
NREL/CP-5400-77082
October 2020

National Renewable Energy Laboratory
15013 Denver West Parkway
Golden, CO 80401
303-275-3000 • www.nrel.gov

NOTICE

This work was authored in part by the National Renewable Energy Laboratory, operated by Alliance for Sustainable Energy, LLC, for the U.S. Department of Energy (DOE) under Contract No. DE-AC36-08GO28308. Funding provided by U.S. Department of Energy Office of Energy Efficiency and Renewable Energy Vehicle Technologies. Office. The views expressed herein do not necessarily represent the views of the DOE or the U.S. Government. The U.S. Government retains and the publisher, by accepting the article for publication, acknowledges that the U.S. Government retains a nonexclusive, paid-up, irrevocable, worldwide license to publish or reproduce the published form of this work, or allow others to do so, for U.S. Government purposes.

This report is available at no cost from the National Renewable Energy Laboratory (NREL) at www.nrel.gov/publications.

U.S. Department of Energy (DOE) reports produced after 1991 and a growing number of pre-1991 documents are available free via www.OSTI.gov.

Cover Photos by Dennis Schroeder: (clockwise, left to right) NREL 51934, NREL 45897, NREL 42160, NREL 45891, NREL 48097, NREL 46526.

NREL prints on paper that contains recycled content.

VALIDATION AND PARAMETRIC INVESTIGATIONS USING A LUMPED THERMAL PARAMETER MODEL OF AN INTERNAL PERMANENT MAGNET MOTOR

Sebastien Sequeira[1], Kevin Bennion[2], J. Emily Cousineau[2], Sreekant Narumanchi[2], Gilbert Moreno[2], Satish Kumar[1], Yogendra Joshi[1]

[1]Georgia Institute of Technology, Atlanta, GA, USA
[2]National Renewable Energy Laboratory, Golden, CO, USA

ABSTRACT

One of the key challenges for the electric vehicle industry is to develop high-power-density electric motors. Achieving higher power density requires efficient heat removal from inside the motor. In order to improve thermal management, a multi-physics modeling framework that is able to accurately predict the behavior of the motor, while being computationally efficient, is essential. This paper first presents a detailed validation of a Lumped Parameter Thermal Network (LPTN) model of an Internal Permanent Magnet (IPM) synchronous motor within the commercially available Motor-CAD® modeling environment. The IPM motor's stator is studied at steady state, and winding losses are generated by a constant DC current. The validation is based on temperature comparison with experimental data and with more detailed Finite Element Analysis (FEA). All critical input parameters of the LPTN are considered in detail for each layer of the stator, especially the contact resistances between the impregnation, liner, laminations and housing. Finally, a sensitivity analysis for each of the critical input parameters is provided. A maximum difference of 4% - for the highest temperature in the slot windings and the end windings - was found between the LPTN and the experimental data. Comparing the results from the LPTN and the FEA model, the maximum difference was 2% for the highest temperature in the slot windings and end windings. As for the LTPN sensitivity analysis, the thermal parameter with the highest sensitivity was found to be the liner-to-lamination contact resistance. The latter is often ignored in the literature, whereas its impact on temperature rise was found to be more significant than any other contact resistance within the stator.

Keywords: Electric motor, thermal management, lumped parameter network, FEA, sensitivity analysis, contact resistances, motor cooling.

INTRODUCTION

With the demand for electric vehicles increasing worldwide, the need for higher-performing electric motors in these vehicles has also become critical. Designing higher-performing electric motors is directly related to these motors having a higher power density. As a result, the U.S. DOE (Department of Energy), as part of the U.S. DRIVE consortium, announced an electric motor power density objective of 50 kW/L for 2025 electric cars [1].

For a long time, research was focused on electromagnetic optimization of electric motors to reach this higher power density. However, thermal constraints due to power losses inside the motor have progressively become a limit for electromagnetic improvements. Electromagnetic and thermal design are interconnected because iron and copper losses from the electromagnetics generate heat and temperature rise inside the motor, leading to a trade-off between the electromagnetics and heat transfer to reach the highest performance [2]. Therefore, overcoming these thermal constraints is now viewed as one of the hardest challenges in meeting the ever-increasing power density objective [3, 4].

In order to overcome the thermal constraints challenge, designers must be able to predict thermal behavior of the electric motor when making design decisions prior to prototyping. This prediction must be accurate enough for selecting the best design solution, and fast enough for exploring the greatest number of solutions. For this prediction, two types of models exist: a full numerical model, usually based on a Finite-Element Analysis (FEA) or Computational Fluid Dynamics/Heat Transfer (CFD/HT), and the analytical model, usually employing a Lumped Parameter Thermal Network (LPTN). CFD/HT and FEA can predict the temperatures with high resolution of a complex geometry but can have high computational costs/time [5], which is not compatible with a fast-iterative design process. Meanwhile, LPTN has a much lower computational cost/time,

but can only predict temperatures for a more limited number of nodes. Although the first LPTN models were quite limited in terms of detailed thermal analysis, more recent densely discretized LPTN models have convinced engineers to adopt these models for the design of electric machines [5]. LPTN model validations have been demonstrated in several papers for both steady-state and transient conditions, and for different types of motors [4, 6-8]. A detailed description of the resistance network for each element of the LPTN based on their geometry and material properties is provided in [7]. More recent work on LPTN models provides an even more spatially resolved discretization especially for the windings [3, 9]. However, limited attention is given to parts of the motor where the material properties strongly depend on the manufacturing processes, such as the liner interface or stator to housing interface.

In this paper, we propose a detailed comparison of an LPTN model with experimental data, along with comparisons with results from an FEA model. This comparison is focused on the stator, as the highest temperatures of an IPM motor are in the windings. Previous work on LPTN validation [7-9] through comparison with experimental data was focused on analyzing individual temperature points, and not on how each part of the stator is contributing to the temperature rise inside the motor. Here we propose a different approach by analyzing temperature profiles along three different paths of the motor, with particular attention to the end-windings region and the different contact interfaces within the stator.

Each thermal parameter of our LPTN is clearly investigated, and a detailed description of how they are related to the thermal parameters of the FEA model is provided. Moreover, a sensitivity analysis of the main thermal parameters is conducted. Through this analysis, we have been able to identify thermal parameters that have the most significant influence on the temperature rise inside the stator, and how this influence is related to future cooling system requirements.

EXPERIMENTAL DATA AND MODELING APPROACH

The Nissan Leaf Electric Motor from Nissan Motor Co. Ltd. will be used as a reference for all geometric, material, and thermal parameters involved in this paper. The main characteristics of this motor are given in Table 1 [10]. The only active cooling system is an external water jacket with 3 circular channels integrated inside an aluminum housing. The coolant used within the water jacket is Water-Ethylene Glycol (WEG).

The present study focuses on thermal analysis of the stator as the IPM motor part subject to the highest temperatures, and where the windings insulation deterioration imposes a significant temperature limit for the motor.

Table 1. Nissan Leaf electric motor features.

Feature	Value
Maximum torque $[N.m]$	280
Maximum power $[kW]$	80
Top speed $[rpm]$	10,390
Weight $[kg]$	58
Volume $[m^3]$	0.019
Number of poles	8
Number of stator slots	48

This paper refers to experimental results available in [11]. For the experiment conducted in [11], the windings were supplied with DC current (voltage of 1.4V and current of 165 amps) and the rotor was removed from the motor. The total heat generated by the windings was 567 W. This was the only heat source. Heat was removed from the windings thanks to convection in the water-jacket cooling system with a coolant flow rate fixed at 10 L/min. Insulation was used to reduce natural convection from the external surfaces directly exposed to ambient air (end-windings, inner stator, housing). Consequently, these surfaces were considered as adiabatic. All boundary conditions are shown in Figure 1.

K-type thermocouples were used for temperature measurements [11]. The different locations of these thermocouples are shown by black and white crosses in Figure 1. All temperature points, from the cross-section plane on Figure 1, except the *Housing* temperature points, are measured in two other cross-section planes rotated by 120° and 240° with respect to the axial direction.

For this paper, we consider that a single temperature label can be attributed to several thermocouples and thus, different temperature points. A set of temperature points with the same label indicates that these should all have the same temperature value based on the assumed symmetry considered for the models presented thereafter. For example, we consider that *End-windings mid* temperature points have the same value for both rear and front end-windings. Similarly, we consider that the *Stator inner face* temperature points have the same temperature along the axial length of the tooth. These assumptions are made in order to have a consistent comparison between experimental data and modeling results.

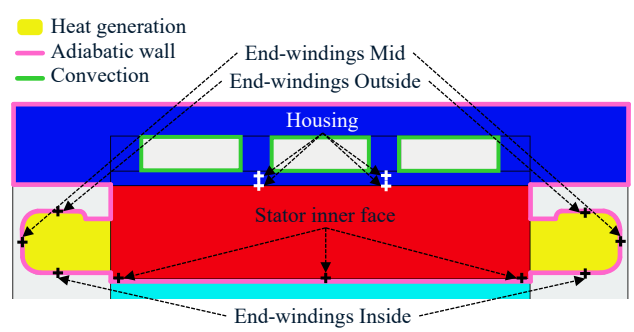

Figure 1. Thermocouples locations on the Leaf motor stator and their associated labels, using Motor-CAD® environment. Heat generation and boundary conditions are shown as well.

It can be noticed that only five different temperatures are considered for these measurements. In fact, inserting thermocouples inside the stator or the windings requires dismantling the laminations or the slot-windings, which would cause a different thermal behavior of the machine. This is one of the main constraints for the validation based on temperature

measurements. Nevertheless, in order to validate the LPTN model with the temperatures inside the stator and the slot-windings, the temperature outputs are compared to the FEA modeling results of the whole stator presented subsequently.

FEA model approach

The FEA model was based on the same motor geometry and thermal properties as the experiments. The same power loss input (567 W) was used. Table 2 gives thermal conductivities for each material involved in the model, thermal contact conductance at each interface and the water-jacket thermal properties. Thermal conductivity and conductance are estimated from the data provided in [12-14]. The water-jacket heat-transfer coefficient is derived from a CFD/HT simulation of the complete water-jacket channels in [11]. The coolant mean temperature value in the water-jacket is also taken from [11]. The tests in [14, 15] were conducted on the Nissan Leaf motor, which makes the evaluation of FEA model thermal parameters more accurate than deducing these from a different motor. We must note that the values for Slot-Windings-to-Liner and Liner-to-Laminations thermal contact conductances are preliminary, requiring further confirmation. Finally, due to the application of thermal insulation, radiation and convection with ambient air are neglected.

Table 2. Thermal conductivities along each direction of a cylindrical system and thermal contact conductance used for the FEA model along with water jacket thermal properties.

Thermal conductivity $[W.m^{-1}.K^{-1}]$			
	Radial	Tangential	Axial
Stator Laminations	21.9	21.9	1.77
Slot-Windings	0.99	0.99	292
End-Windings	0.76	202	101
Slot liner	0.18	0.18	0.18
Aluminum	167	167	167
Thermal contact conductance $[W.m^{-2}.K^{-1}]$			
Slot-Windings | Liner			556
Liner | Laminations			1645
Laminations | Housing			5555
Water-jacket cooling system			
Heat transfer coefficient $[W.m^{-2}.K^{-1}]$			1428
Flow rate $[L.min^{-1}]$			10.0
Coolant mean temperature [°C]			65

Two screenshots of the mesh are shown in Figure 2. For our FEA model, the average mesh size was chosen to be 2.7 mm. This choice was based on a mesh independence study where computing time and maximum temperature with respect to mesh size were derived (see Figure 3). Red labelled markers in Figure 3 correspond to the final average mesh size of the FEA model. With this final mesh size of 2.7 mm, the numerical results are accurate to within 0.4%.

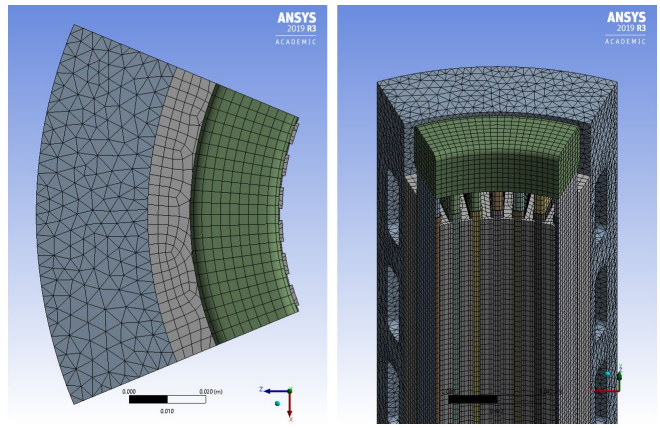

Figure 2. Mesh of the FEA model (average size of 2.7 mm).

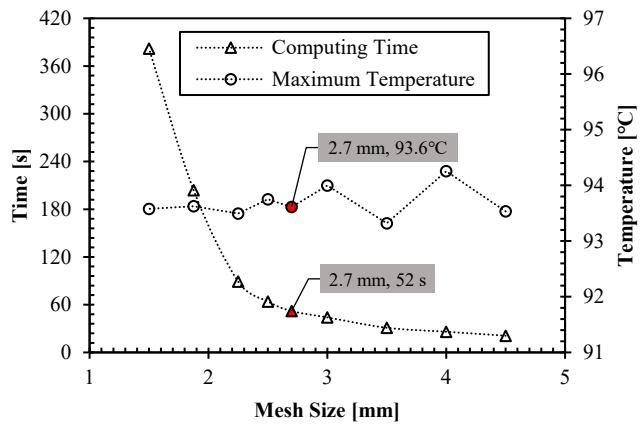

Figure 3. Computing time and maximum temperature of the FEA model with respect to mesh size.

Lumped Parameter Thermal Network model approach

The LPTN model was created using Motor-CAD® software environment, where the electric motor geometry is designed first. In order to have dimensions as close as possible to that of the real motor, dimensions from the FEA geometric model have been used. The resulting geometry can be seen in Figure 4: the radial view of the motor is represented on the left, and the axial view on the right. The LPTN is directly associated with this geometry and a simplified representation is given in Figure 5. In this paper, we are only analyzing the thermal behavior of the stator. LPTN resistances that are connecting any stator nodes to the rotor or ambient air are consequently considered as infinite resistances. Thus, the inner tooth wall is assumed to be adiabatic. In the LPTN, each part with a given material property, and each interface are represented by a resistance. Each node of the network represents a temperature and the sources of the circuit correspond to the copper losses generated inside the windings (567 W). Each of these parameters is described in detail in the subsequent paragraphs.

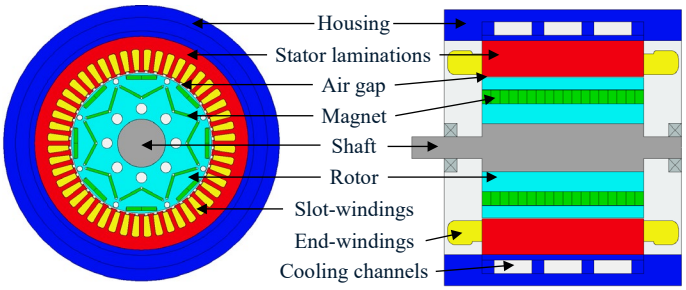

Figure 4. Nissan Leaf motor geometry within Motor-CAD® environment: radial cross-section view on the left, axial cross-section view on the right.

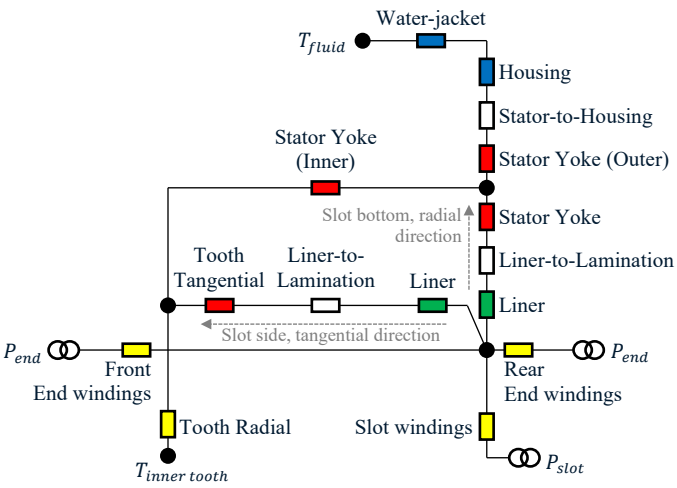

Figure 5. Simplified representation of the stator LPTN model (based on Motor-CAD® schematic).

Power loss distribution

Here, we are considering only DC current which means no core losses or eddy current losses, as the magnetic field is not time dependent. Therefore, the only considered losses P are the copper losses generated by the DC current in the windings equal to 567 W, from the experiments. Besides, P is split between slot-windings and end-windings, with respect to their volume, which yields (1) and (2):

$$P_{slot} = \alpha P$$
$$P_{end} = \frac{1}{2}(1-\alpha)P \quad (1)$$
$$\alpha = \frac{\mathcal{V}_{slot}}{\mathcal{V}_{slot}+2\mathcal{V}_{end}} \quad (2)$$

Where $\mathcal{V}_{slot}$ is the total volume of slot-windings, $\mathcal{V}_{end}$ is the volume of each end-windings (the rear and front end-windings of the motor are considered to have the same volume), P_{slot} is the fraction of P generated inside $\mathcal{V}_{slot}$, P_{end} is the fraction of P generated inside $\mathcal{V}_{end}$, and α is the volume ratio between slot-windings and end-windings.

From equation (1) and (2), it can be noticed that knowing α and P, one can define both P_{slot} and P_{end} which are used as the power loss sources within the LPTN. Here, $\alpha = 19\ \%$ and $P = 567\ W$. As a result, P and α are the parameters that are used as inputs to Motor-CAD® which then computes P_{slot} and P_{end} for the LPTN giving: $P_{slot} = 351.5\ W$ and $P_{end} = 107.7\ W$.

Stator lamination thermal conductivity

Stator laminations are composed of successive layers of silicon steel (also called electrical steel) sheets separated by a thin layer of coating material which forms the inter-lamination layer. In fact, this coating material is not a single material but a surface treatment of steel sheets, which makes the prediction of its equivalent conductivity k_{int}, and thus its thermal implications, very difficult [12]. In order to derive k_{int}, it has been expressed as a function of stator stack equivalent thermal conductivities whose values are given in Table 2. Next paragraphs show how this expression has been derived.

A cross-sectional view of the stator laminations is shown in Figure 6. The laminations are positioned within (X,Y) plane normal to the axial direction of the motor (Z-axis in Figure 6). Steel sheets and inter-laminations are characterized by their thermal resistance in each direction which are derived from their thermal conductivities, k_{steel} and k_{int} respectively, and cross-sectional areas normal to the respective direction. Based on the notations used in Figure 6, thermal resistances are defined as:

$$X \rightarrow R_{steel_X} = \frac{l}{k_{steel}A_{steel_X}}, R_{int_X} = \frac{l}{k_{int}A_{int_X}} \quad (3)$$
$$Z \rightarrow R_{steel_Z} = \frac{e_{steel}}{k_{steel}A_Z}, R_{int_Z} = \frac{e_{int}}{k_{int}A_Z} \quad (4)$$

Where R_{steel_X}, R_{steel_Z}, A_{steel_X}, A_Z are the steel sheet resistances and cross-sectional areas normal to the X and Z directions, respectively, and R_{int_X}, R_{int_Z}, A_{int_X} are interlamination resistances and cross-sectional areas normal to the X and Z directions, respectively. Note that the Y direction is not considered as equations and conclusions are the same as for the X direction due to inherent symmetry.

Two other useful dimensions must be defined:

$$A_X = nA_{steel_X} + (n-1)A_{int_X} \quad (5)$$
$$L = ne_{steel} + (n-1)e_{int} \quad (6)$$

Where A_X is the total cross-sectional area of the stator stack normal to X, L is the total length of the stator stack along Z and n is the number of steel sheets.

Along the X direction, thermal resistances between each layer are in parallel whereas along the Z direction, thermal resistances are in series, as shown in Figure 6. As a result, equations (7) and (8) give an expression for the stator stack equivalent thermal resistances R_X and R_Z respectively.

$$\frac{1}{R_X} = \frac{n}{R_{steel_X}} + \frac{n-1}{R_{int_X}} \quad (7)$$
$$R_Z = nR_{steel_Z} + (n-1)R_{int_Z} \quad (8)$$

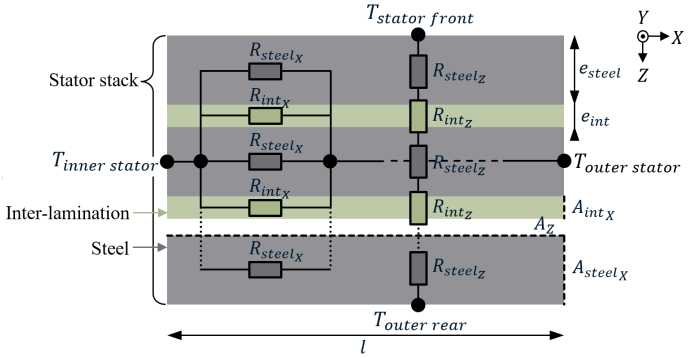

Figure 6. Stator laminations cross-section view where Z-axis is along the axial direction of the stator.

Stator stack equivalent thermal conductivities k_X (along X) and k_Z (along Z) can be expressed as a function of R_X and R_Z respectively:

$$k_X = \frac{l}{R_X A_X} \tag{9}$$

$$\frac{1}{k_Z} = \frac{R_Z A_Z}{L} \tag{10}$$

Finally, the stacking factor S_f, known as the relative cross-sectional area of silicon steel to the overall cross-sectional area of stator laminations, can be expressed with respect to geometric parameters from Figure 6:

$$S_f = \frac{nA_{steel_X}}{A_X} = \frac{ne_{steel}}{L} \tag{11}$$

For the Nissan Leaf electric motor stator, $S_f = 0.97$ [15]. Combining equations (3), (5), (7), (9), (11) yields equation (12) and combining (4), (6), (8), (10), (11) yields (13) below. Again, due to symmetry reasons, we have $k_X = k_Y$.

$$k_X = k_Y = S_f \times k_{steel} + (1 - S_f) \times k_{int} \tag{12}$$

$$\frac{1}{k_Z} = \frac{S_f}{k_{steel}} + \frac{1 - S_f}{k_{int}} \tag{13}$$

In Motor-CAD®, k_{steel} and k_{int} are used as input values. k_{steel} and k_{int} are derived from (12) and (13) with respect to k_X, k_Y and k_Z values. In order to have a consistent comparison with the FEA model, k_X, k_Y and k_Z values are taken from Table 2. Solving (12) and (13) for k_{int} and k_{steel}, we obtain input values that are used for our LPTN:

$$\begin{cases} k_{int} = 0.054\ W.m^{-1}.°C^{-1} \\ k_{steel} = 23\ W.m^{-1}.°C^{-1} \end{cases}$$

Slot-windings equivalent thermal conductivity

The copper wires used for the windings have a diameter $D_c = 0.800\ mm$ and a total diameter (including insulation) $D = 0.885\ mm$. Maximizing the number of wires which can fit inside a single slot of the Leaf motor leads to a maximum copper slot fill of 52%.

Within the LPTN, the slot-windings are defined as a set of cuboids which includes both windings and impregnation material. These cuboids are the rectangles represented in Figure 7(b). As it may be observed, each cuboid has its own height and width, whereas they all have the same axial length corresponding to the length of active windings, namely the length of the stator. These cuboids allow to simplify the slot-windings model. Each cuboid can be represented as shown in Figure 7(a). The node in the center of the cuboid represents the average temperature T_C of the cuboid. Each face of the cuboid includes a node connected to the rest of the LTPN. The face nodes are also connected to the central node by resistances accounting for the heat transfer from the center of the cuboid to each of its faces (they are not represented here). Copper losses are represented by a heat source located at the central node T_C. Here, as shown in Figure 7(b), there are two sets of 10 cuboids on each side of the slot. We can notice that these two sets are symmetric with respect to the midline of the slot. Then, we assume that temperatures will be symmetric with respect to this midline. This set of 10 cuboids is represented by a single yellow resistor labelled *Slot winding* on Figure 5.

The value of each resistance connecting the face nodes and the center node is derived from the equivalent thermal conductivities along X, Y and Z. In order to fairly compare LPTN results with the FEA modeling results, we chose user defined equivalent thermal conductivities coming from the FEA model as input data given in Table 2. This type of segmentation with a high number of cuboids is used in recent thermal modeling of electric machines [3, 9].

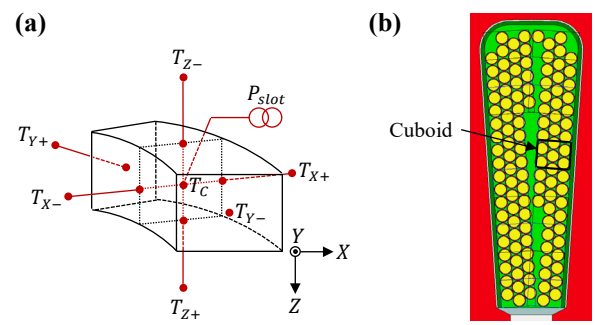

Figure 7. Slot-windings cuboids: (a) 3D model representation, (b) in-plane representation within Motor-CAD® environment.

End-windings equivalent thermal conductivity

As for the FEA model, end-windings are considered as a single toroid, which does not account for contact resistance between each of the end-turns. This simplification is considered accurate enough to give a good approximation for end-windings thermal analysis. Besides, end-windings modeling in the LPTN follows the same model as that of the slot-winding. Thus, end-winding blocks will be divided into 10 cuboids. Each of these cuboids from the end-windings will be connected to the slot-windings cuboids on their $T_{Z\pm}$ nodes. By default, in Motor-CAD®, cuboid thermal conductivities along X, Y and Z directions for both end-windings and slot-windings have the same values. However, in the end-windings, as each wire forms

a loop from one slot to another, the highest thermal conductivity is along the tangential direction. As a result, tangential thermal conductivity should be much higher in the end-windings than in the slot-windings. The FEA model accounts for this thermal conductivity difference between end-windings and slot-windings (see Table 2). Moreover, FEA and LPTN models must be accurately compared which encourages us to choose user-defined values of end-winding thermal conductivities, based on data from Table 2.

Stator-to-housing thermal conductance

Thermal contact resistances are also very important for the LPTN model, as they represent the largest uncertainties due to manufacturing processes [2]. For example, the stator external surface roughness significantly affects the effective thermal conductance between the stator lamination and the housing [13]. Usually, to account for this roughness, a stator-to-housing mean gap is employed. A usual mean gap which corresponds to a good contact between the laminations and the housing is around $0.01\,mm$ [16], giving a corresponding stator-to-housing conductance of $3{,}171\ W.m^{-2}.°C^{-1}$ for the Leaf motor.

For our LPTN, we must use the same thermal conductance as that from the FEA model, namely $5{,}555\ W.m^{-2}.°C^{-1}$ from Table 2. This thermal conductance corresponds to a mean gap of $0.006\ mm$. It would suggest that the stator-to-housing contact for the Nissan Leaf motor is better than usual good contact values provided in [16]. Nevertheless, this suggestion must be used carefully, as the value from the FEA model in Table 2 was derived from a temperature measurement based on a sample of stator laminations, and not directly on the motor [13].

Slot-liner contact

Slot-liner contact resistance accounts for the contact with windings (in fact, with impregnation material) and with laminations. This thermal resistance is caused by several manufacturing and assembly processes which yield imperfections, along with high uncertainties in the measured value of this resistance [17]. The accurate prediction of the thermal contact resistance has been proven to be highly critical in the prediction of the machine thermal behavior [16, 17].

Usually, instead of contact resistance, we use the contact conductance. Therefore, for the liner contact area, we have a conductance for the winding side $G_{Liner-Wdg}$ and the conductance for the lamination side $G_{Liner-Lam}$ which form the equivalent thermal contact conductance of the liner G_{Liner}:

$$G_{Liner} = \left(\frac{1}{G_{Liner-Lam}} + \frac{1}{G_{Liner-Wdg}}\right)^{-1} \qquad (14)$$

In Motor-CAD®, in order to represent the equivalent thermal contact resistance for the liner, an impregnation layer is considered between the liner and the laminations. The impregnation thermal conductivity combined with a goodness factor can represent the thermal conductance defined in (14). Thus, the thermal resistance related to G_{Liner} is, in fact, from the LPTN perspective, the equivalent resistance of a 0.1 mm layer of impregnation between the liner and the stator lamination multiplied by a goodness factor of 0.051. The very low value of this goodness factor shows that considering a perfect contact with the liner is questionable if an accurate LPTN is required. Indeed, in the real motor, the contact is not perfect at all, hence the low thermal conductance of the liner measured in [18] and given in Table 2.

Reasons for low thermal conductance of liner contact can be numerous. First, the roughness of the lamination as well as that of the liner enhance the contact resistance between the liner and the laminations. Second, the windings impregnation is not perfect and thus, air bubbles can remain between the windings and the liner: contact goodness can, thus, deteriorate. Third, there is no additional pressure on the liner that would improve the effective contact area with the laminations or the windings.

In , two resistors are associated with the liner-to-lamination contact resistance: one is for the contact with tooth slot side and the other is for the contact with slot bottom.

RESULTS AND DISCUSSION

Temperature results from experiments, FEA model and LPTN model are compared and discussed first. In the second part, a sensitivity analysis of each main thermal resistance from the LPTN is presented and discussed.

LPTN model and experimental data

After performing the LPTN simulations, we compared in Figure 8 the temperatures from experiments and the LPTN at the same locations. Labels used for each bar in Figure 8 come from Figure 1. The same reference temperature of 65 °C (coolant mean temperature) is used for both LPTN and experiments. As a reminder from Figure 1, one temperature corresponds to the average at different points, from symmetry considerations. Thus, one can derive the standard deviation for each of the five labeled temperatures in Figure 8. These standard deviations are represented by error bars in Figure 8. Standard deviations for each temperature associated with the end-windings are larger than for the *Housing* or the *Stator inner face*. Whereas the housing or the stator can be considered as orthotropic materials, end-windings are made of several bent wires with various trajectories assembled with impregnation which can contain air bubbles. Moreover, there are non-equal spaces between end-turns. Therefore, end-windings are highly anisotropic and the assumed symmetry along the tangential direction of the end-windings implies these larger standard deviations.

In order to compare LPTN and experimental results, we can compute the relative error between LPTN and experimental results for each temperature. End-windings suffer from the highest relative error. Indeed, characterizing end-windings as a single toroid involves significant simplifications as, in the real end-windings, there are three layers of end-turns along the radial axis accounting for the three phases. In these end-turns, wires are curved to go from one slot to another and create a loop which makes the thermal conductivity of end-windings highly position-

dependent. As a result, considering a fixed thermal conductivity along each axis of a cylindrical coordinate system in a single toroid is a strong simplification compared to real end-windings. Consequently, this yields the temperature differences between the LPTN and the experiments. Despite all these simplifications, we obtain a maximum relative error of 3.6% which demonstrates a good agreement between experimental data and LPTN results. Accordingly, we can claim that the LPTN model is able to accurately predict the steady-state temperatures of the Nissan Leaf motor.

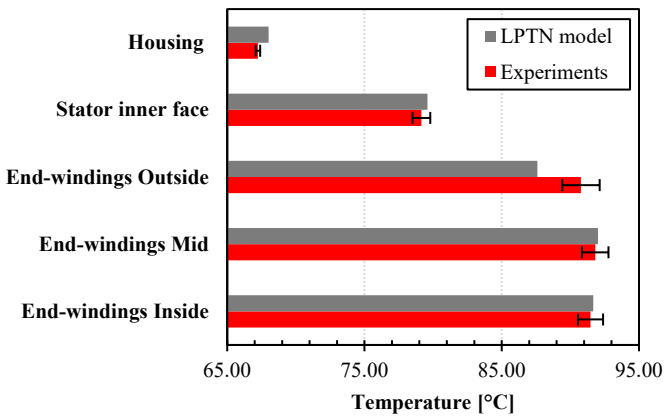

Figure 8. Measured temperatures compared to LPTN output temperatures at 5 different points of the stator. Coolant mean temperature of 65 °C is used for both LPTN and experiments.

LPTN model and FEA model

The results from the FEA steady-state thermal analysis are shown in Figure 9. The comparison between LPTN and FEA models relies on temperature profiles along three different paths represented in Figure 10. Path (1) crosses the slot-windings and stops at the cooling channel wall, path (2) crosses the tooth and stops at the cooling channel wall and path (3) crosses the mid plane of the end-windings along the radial direction.

In order to have a better visualization for the comparison, temperature profiles from FEA and LPTN are given in Figure 11 for path (1), Figure 12 for path (2) and Figure 13 for path (3). For each of these figures, temperatures from experiments (see Figure 8) have also been reported. As presented in the previous section, LPTN representation of windings is based on cuboid structure. For Figure 11 and Figure 13, the cuboid temperature node which was used for the plots is T_c (see Figure 7), namely the temperature of the cuboid's center node. In order to have an idea of temperature extremum for each cuboid, the maximum and minimum temperature envelope has been plotted as grey dotted lines on both Figure 11 and Figure 13. These envelopes are associated with the cuboid model in the LPTN which is only used for windings, thus, the dotted line is plotted only for the slot-windings part on Figure 11. Looking at the domain between these two envelopes is more relevant when comparing the LPTN model to experimental data or FEA model since the plot of T_C temperature does not correspond necessarily to the exact same temperature point in the FEA model or in the experiments.

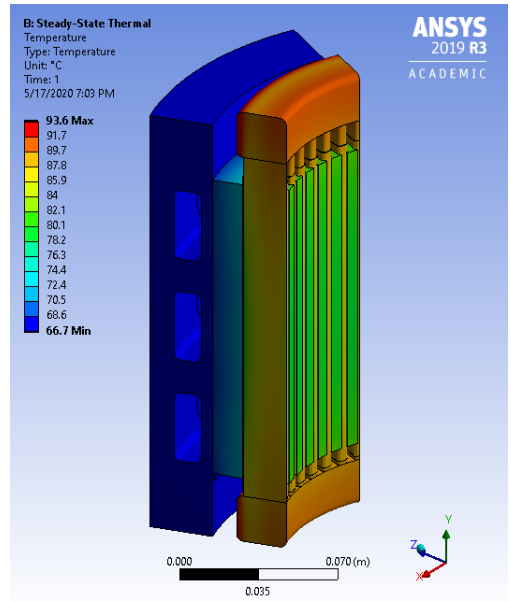

Figure 9. Stator temperatures from FEA steady-state thermal simulation.

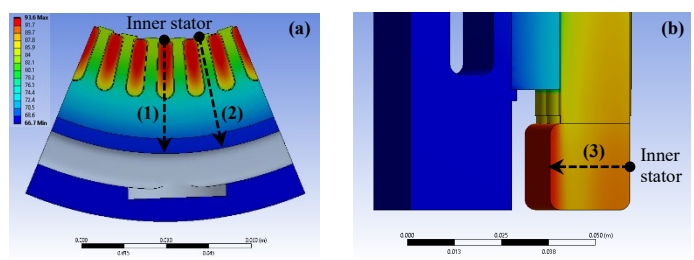

Figure 10. Temperature profile paths: (a) path (1) and path (2) locations in the midplane cross-section view of the stator and (b) path (3) location in the axial cross-section view of the stator.

The maximum relative error between LPTN and FEA models for each path is given in Table 3. The overall maximum relative error is about 2% which makes the LPTN highly consistent with the FEA results for the regions where we have critical temperatures in a motor, namely slot-windings, stator tooth and end-windings. This confirms the ability of the LPTN to replace an FEA model for steady-state thermal analysis of an electric machine. The computational time for the LPTN steady-state analysis is about 4 seconds, whereas the FEA computational time, with the same computer configuration, is about 52 seconds. However, the LPTN inherent structure provides far coarser temperature resolution than the FEA model.

Thermal design of an electric motor is mainly focused on the highest temperature in each of its parts. Indeed, especially for the stator, the thermal limit is fixed by the temperature limit of the windings due to the wire insulation deterioration. As a result, having a number of temperature points is not essential as long as the maximum temperature values in each part are accurately

predicted. The accuracy has been shown to be significantly high especially along path (2). For this path, we are only crossing stator laminations and the housing. Stator laminations can be accurately model within a LPTN as they are composed of steady distributed silicon iron sheets.

Table 3. Maximum relative error between FEA and LPTN model temperature profiles

Path	Error
(1) → slot-windings	0.95 %
(2) → stator tooth	0.52 %
(3) → end-windings	2.08 %

The highest error occurs in the end-windings (Figure 13). We have already discussed the difference between end-windings LPTN model with a single toroid and fixed orthotropic thermal conductivity and the real end-windings in *LPTN model and experimental data* section. The FEA model also uses a single toroid and fixed orthotropic thermal conductivity; however, the LPTN and FEA temperature profiles are reversed in the region beyond 17 mm from the inner stator.

The reason for this temperature rise in the FEA model comes from the low radial thermal conductivity value compared to the axial, and tangential thermal conductivities in the end-windings, see Table 2. For a more detailed explanation, end-windings volume can be represented as a combination of two volumes $\mathcal{V}_1$ and $\mathcal{V}_2$ as shown in Figure 14. Here $\mathcal{V}_2$ is the volume beyond 17 mm. As can be noticed in Figure 14, the heat flux q_2 from $\mathcal{V}_2$ to $\mathcal{V}_1$ occurs along the radial direction and unlike $\mathcal{V}_1$, $\mathcal{V}_2$ is not directly connected to the slot-windings. As a result, the heat produced in $\mathcal{V}_2$ leaves through surface A_2 (convection is neglected). Yet, the thermal conductivity along the radial direction is much lower than that along the axial direction – direction of heat flux q_1 from $\mathcal{V}_1$ to the slot-windings. This results in a temperature increase in $\mathcal{V}_2$ away from A_2 in the radial direction. However, from Figure 13, the temperature is decreasing within $\mathcal{V}_2$ for the LPTN model. Indeed, as for the slot-windings, end-windings are represented as a set of cuboids within the LPTN model, each connected to the slot-windings cuboids on their $T_{Z\pm}$ nodes (see Figure 7). It means all cuboids are directly connected to the slot-windings, and thus, there is no equivalent volume $\mathcal{V}_2$, as for the FEA, which is not directly connected to the end-windings. Within the LPTN, the end-windings are represented as a single volume $\mathcal{V}_1$. This explains why LPTN temperature profile is still decreasing as we go beyond the bottom of the slot-winding.

Eventually, in Figure 13, the LPTN predictions are closer to the experiments. This is consistent since all wires that are in volume $\mathcal{V}_2$ come from the slot-windings. Thus, in the real end-windings, heat flux follows the curved path of the wires which make volume $\mathcal{V}_2$ directly connected to the slot-windings, hence the lower temperatures experimentally observed outside of the windings.

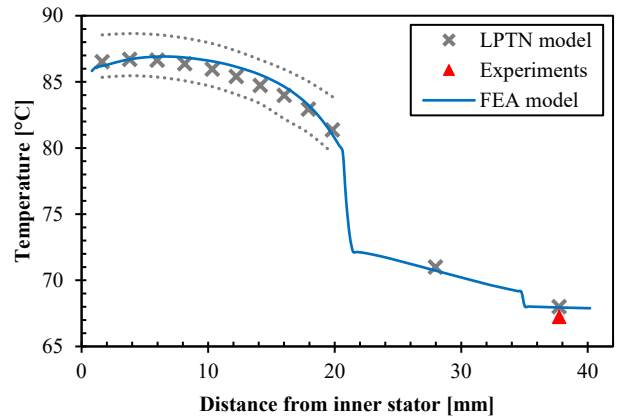

Figure 11. Temperature profiles along a slot following path (1). Profiles are given for the FEA model, LPTN model and experimental data.

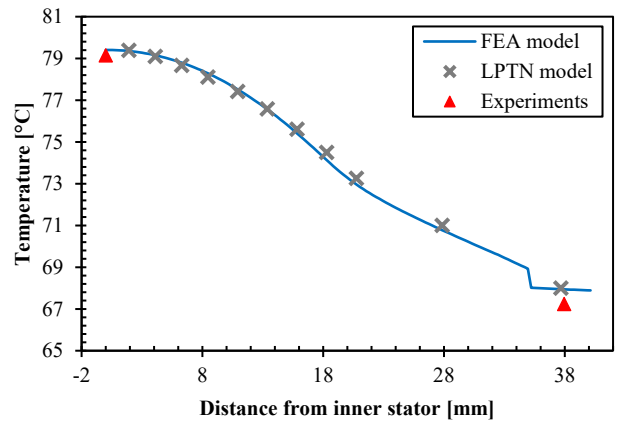

Figure 12. Temperature profiles along a tooth following path (2). Profiles are given for the FEA model, LPTN model and experimental data.

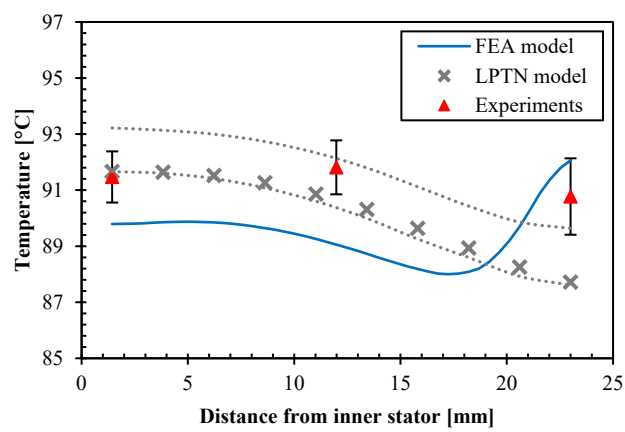

Figure 13. Temperature profiles along end-windings following path (3). Profiles are given for the FEA model, LPTN model and experimental data.

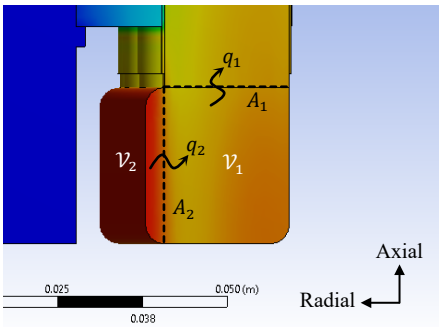

Figure 14. End-windings heat flux and volume separation.

Sensitivity analysis

A sensitivity analysis using the LPTN can help identify the resistances most responsible for the temperature rise in the stator [19]. Usually, for a sensitivity analysis the thermophysical properties of the different materials are considered [20]. However, because both thermal conductances and thermal conductivities are considered here, the present sensitivity analysis is based on their equivalent thermal resistance. The final thermal parameters and their associated thermal resistance names chosen for the present sensitivity analysis are given in Table 4.

Table 4. List of thermal resistances used for the sensitivity analysis, and their related initial thermal parameter.

Thermal resistance	Associated thermal parameter
R [Liner Contact]	Liner-to-lamination thermal contact conductance
R [Liner]	Liner thermal conductivity
R [Slot-Windings]	Slot-windings equivalent thermal conductivity
R [Water-Jacket]	Channels heat transfer coefficient
R [Housing Contact]	Housing-to-lamination thermal contact conductance
R [Housing]	Housing thermal conductivity

The LPTN used for the sensitivity analysis was based on a 20% and 50% value reduction for each thermal resistance in Table 4. The sensitivity was assessed by computing the temperature difference ΔT between the winding maximum temperature with initial resistances and the winding maximum temperature with the new reduced resistance. Figure 15 presents the results of the sensitivity analysis for each resistance and each percentage reduction.

Figure 15 shows that the *Liner Contact* resistance has the highest influence on the temperature variation of the motor, followed by the *Liner* resistance. This high influence of the liner relates to the highest temperature decrease (≈ 7°C), at 21 mm from the inner stator in Figure 11. This temperature decrease occurs along a very short distance, less than 1 mm, corresponding to the liner area.

The liner influence is due to the low thermal conductivity of the liner compared to other thermal conductivities involved (see Table 2). Also, this influence comes from the low contact thermal conductance of the liner compared to other thermal conductances like the stator-to-housing contact conductance. Although the difference between contact thermal conductance of the liner compared to other conductances seems quite high, it remains consistent. Indeed, stator-to-housing thermal resistance is essentially caused by laminations roughness. At the lamination-to-liner interface, this same roughness is responsible for a decrease in the contact conductance. However, imperfections during impregnation process, as well as remaining air between the liner and the laminations significantly impact further reduction of the liner contact conductance.

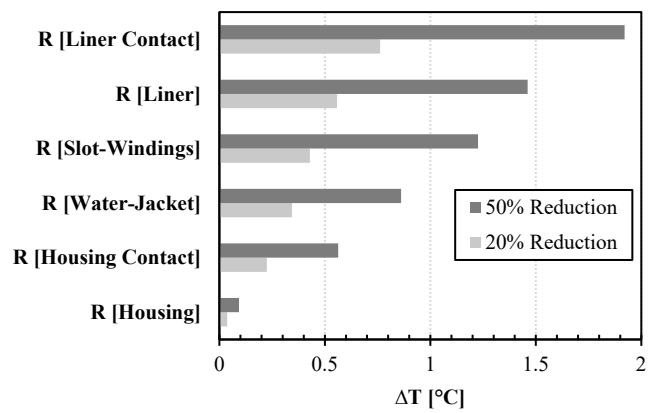

Figure 15. Sensitivity analysis of the LPTN thermal resistances for 20 % and 50 % value reductions.

It is worth noticing that *Water-Jacket* resistance sensitivity is less than half of the *Liner Contact* resistance sensitivity. This shows that improving the heat transfer coefficient of a cooling jacket system outside of the slot-windings has some limitations in terms of maximum temperature reduction. This is particularly illustrated in Figure 16. The limitation of increasing the heat transfer coefficient is represented by the dashed line asymptote equal to 91.50 °C. Therefore, the maximum temperature difference between the current heat transfer coefficient ($1{,}428\ W.m^{-2}.°C^{-1}$) and an infinite heat transfer coefficient is about 1.7 °C.

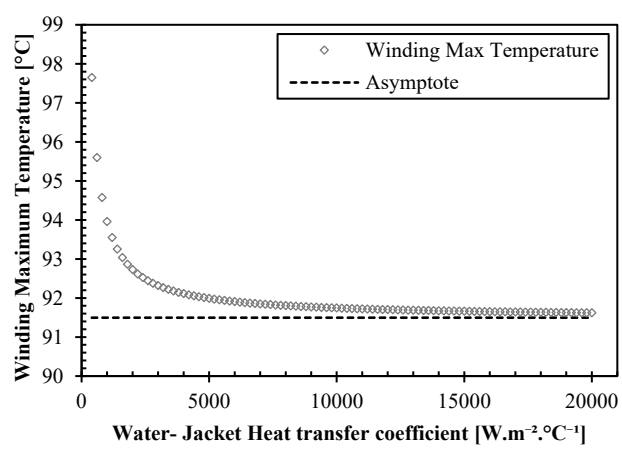

Figure 16. Winding maximum temperature as a function of water-jacket heat transfer coefficient. Results are computed with our LPTN model.

From the previous observations, we can draw an important conclusion. The next-generation cooling systems that will make IPM motors reach high power densities must be between the liner and the windings. According to the sensitivity analysis, improving the water-jacket heat transfer coefficient or the stator-to-housing conductance will not provide enough temperature decrease in the windings. Thus, creating direct cooling of the windings with a focus on end-windings, as end-windings are subject to the maximum temperature, seems inevitable for reaching significantly higher power densities.

CONCLUSIONS

In this paper, we have first proposed a detailed comparison of an LPTN model with experimental data for steady-state thermal analysis of the Nissan Leaf motor stator. The maximum temperature difference between LPTN and experimental temperatures was under 4%. The LPTN model was also compared to an FEA model, with a maximum difference of 2%. End-windings were found to be a critical region in terms of modeling accuracy. Temperature profile differences have been explained in detail, especially for the end-windings outside region extending beyond the bottom of the slots.

Finally, a sensitivity analysis was conducted for six thermal resistances involved in the LPTN model. Liner contact resistance had the highest influence. Comparing influences of other thermal resistances shows that improving heat transfer coefficient of a cooling system outside of the stator does not provide significant temperature reduction of the windings. Creating a very high-power-density electric motor will require having a cooling system inserted between the liner and the winding.

ACKNOWLEDGMENTS

This material is based upon work supported by the U.S. Department of Energy's Office of Energy Efficiency and Renewable Energy (EERE) under the Vehicle Technologies Program Office Award Number DE-EE0008708. The authors would like to particularly acknowledge Amitav Tikadar for help with LPTN modeling within Motor-CAD® environment.

DISCLAIMER

REFERENCES

[1] "Electrical and Electronics Technical Team Roadmap," U.S. Driving Research and Innovation for Vehicle efficiency and Energy sustainability, 2017.

[2] D. Staton, A. Boglietti, and A. Cavagnino, "Solving the more difficult aspects of electric motor thermal analysis in small and medium size industrial induction motors," *IEEE Transactions on Energy Conversion,* vol. 20, no. 3, pp. 620-628, 2005, doi: 10.1109/TEC.2005.847979.

[3] V. Madonna, A. Walker, P. Giangrande, G. Serra, C. Gerada, and M. Galea, "Improved Thermal Management and Analysis for Stator End-Windings of Electrical Machines," *IEEE Transactions on Industrial Electronics,* vol. 66, no. 7, pp. 5057-5069, 2019, doi: 10.1109/TIE.2018.2868288.

[4] M. Popescu, D. A. Staton, A. Boglietti, A. Cavagnino, D. Hawkins, and J. Goss, "Modern Heat Extraction Systems for Power Traction Machines—A Review," *IEEE Transactions on Industry Applications,* vol. 52, no. 3, pp. 2167-2175, 2016, doi: 10.1109/TIA.2016.2518132.

[5] A. Boglietti, A. Cavagnino, D. Staton, M. Shanel, M. Mueller, and C. Mejuto, "Evolution and Modern Approaches for Thermal Analysis of Electrical Machines," *IEEE Transactions on Industrial Electronics,* vol. 56, no. 3, pp. 871-882, 2009, doi: 10.1109/TIE.2008.2011622.

[6] Q. Chen, Z. Zou, and B. Cao, "Lumped-parameter thermal network model and experimental research of interior pmsm for electric vehicle," *CES Transactions on Electrical Machines and Systems,* vol. 1, no. 4, pp. 367-374, 2017, doi: 10.23919/TEMS.2017.8241358.

[7] P. H. Mellor, D. Roberts, and D. R. Turner, "Lumped parameter thermal model for electrical machines of TEFC design," *IEE Proceedings B - Electric Power Applications,* vol. 138, no. 5, pp. 205-218, 1991, doi: 10.1049/ip-b.1991.0025.

[8] A. M. E.-. Refaie, N. C. Harris, T. M. Jahns, and K. M. Rahman, "Thermal analysis of multibarrier interior PM synchronous Machine using lumped parameter model," *IEEE Transactions on Energy Conversion,* vol. 19, no. 2, pp. 303-309, 2004, doi: 10.1109/TEC.2004.827011.

[9] H. Zhang *et al.*, "Thermal Model Approach to Multisector Three-Phase Electrical Machines," *IEEE Transactions on Industrial Electronics,* vol. PP, pp. 1-1, 03/06 2020, doi: 10.1109/TIE.2020.2977559.

[10] Y. Sato, S. Ishikawa, T. Okubo, M. Abe, and K. Tamai, "Development of High Response Motor and Inverter System for the Nissan LEAF Electric Vehicle," 2011. [Online]. Available: https://doi.org/10.4271/2011-01-0350.

[11] G. Moreno, "Thermal Performance Benchmarking: Annual Report,"; National Renewable Energy Lab. (NREL), Golden, CO (United States), NREL/MP-5400-64941 United States 10.2172/1247461 NREL English, 2016. [Online]. Available: https://www.osti.gov/servlets/purl/1247461

[12] J. E. Cousineau, K. Bennion, D. DeVoto, and S. Narumanchi, "Experimental characterization and modeling

of thermal resistance of electric machine lamination stacks," *International Journal of Heat and Mass Transfer,* vol. 129, pp. 152-159, 2019/02/01/ 2019, doi: https://doi.org/10.1016/j.ijheatmasstransfer.2018.09.051.

[13] J. Emily Cousineau, K. Bennion, V. Chieduko, R. Lall, and A. Gilbert, "Experimental Characterization and Modeling of Thermal Contact Resistance of Electric Machine Stator-to-Cooling Jacket Interface Under Interference Fit Loading," *Journal of Thermal Science and Engineering Applications,* vol. 10, no. 4, 2018, doi: 10.1115/1.4039459.

[14] A. A. Wereszczak *et al.*, "Anisotropic Thermal Response of Packed Copper Wire," *Journal of Thermal Science and Engineering Applications,* vol. 9, no. 4, 2017, doi: 10.1115/1.4035972.

[15] "Modelling the Nissan Leaf Motor using Motor-CAD," Motor Design Ltd., 2019. [Online]. Available: https://www.motor-design.com/publications/tutorials/

[16] A. Boglietti, A. Cavagnino, and D. Staton, "Determination of Critical Parameters in Electrical Machine Thermal Models," *IEEE Transactions on Industry Applications,* vol. 44, no. 4, pp. 1150-1159, 2008, doi: 10.1109/tia.2008.926233.

[17] R. Wrobel, S. J. Williamson, J. D. Booker, and P. H. Mellor, "Characterizing the in situ Thermal Behavior of Selected Electrical Machine Insulation and Impregnation Materials," *IEEE Transactions on Industry Applications,* vol. 52, no. 6, pp. 4678-4687, 2016, doi: 10.1109/tia.2016.2589219.

[18] K. Bennion, "Electric Motor Thermal Management R&D. Annual Report,"; National Renewable Energy Lab. (NREL), Golden, CO (United States), NREL/MP-5400-64944 United States 10.2172/1248569 NREL English, 2016. [Online]. Available: https://www.osti.gov/servlets/purl/1248569

[19] A. Boglietti, A. Cavagnino, and D. A. Staton, "TEFC induction motors thermal models: a parameter sensitivity analysis," in *Conference Record of the 2004 IEEE Industry Applications Conference, 2004. 39th IAS Annual Meeting.*, 3-7 Oct. 2004 2004, vol. 4, pp. 2469-2476 vol.4, doi: 10.1109/IAS.2004.1348822. [Online]. Available: https://ieeexplore.ieee.org/document/1348822/

[20] K. Bennion and J. Cousineau, "Sensitivity analysis of traction drive motor cooling," in *2012 IEEE Transportation Electrification Conference and Expo (ITEC)*, 18-20 June 2012 2012, pp. 1-6, doi: 10.1109/ITEC.2012.6243512. [Online]. Available: https://ieeexplore.ieee.org/document/6243512/